` **Integration of Activating and Inhibitory Receptor Signaling by Regulated Phosphorylation of Vav1 in Immune Cells**

Sven Mesecke, Doris Urlaub, Hauke Busch, Roland Eils and Carsten Watzl (31 May 2011)

Science Signaling **4** (175), ra36. [DOI: 10.1126/scisignal.2001325]

COMPUTATIONAL BIOLOGY

Integration of Activating and Inhibitory Receptor Signaling by Regulated Phosphorylation of Vav1 in Immune Cells

Sven Mesecke,[1,2*] Doris Urlaub,[2*] Hauke Busch,[1†] Roland Eils,[1,3‡] Carsten Watzl[2‡§]

Natural killer (NK) cells are effector cells of the immune system whose activation is carefully regulated by the interplay of signals from activating and inhibitory receptors. Signals from activating receptors induce phosphorylation of the guanine nucleotide exchange factor Vav1, whereas those from inhibitory receptors lead to the dephosphorylation of Vav1 by the Src homology 2 domain–containing protein tyrosine phosphatase 1 (SHP-1). Here, we used mathematical modeling and experiments with NK cells to gain insight into this integration of positive and negative signals at a molecular level. Our data showed a switch-like regulation of Vav1 phosphorylation, the extent of which correlated with the cytotoxic activity of NK cells. Comparison of our experimental results with the predictions that we derived from an ensemble of 72 mathematical models showed that a physical association between Src family kinases and activating receptors on NK cells was essential to generate the cytotoxic response. Our data support a central role for Vav1 in determining the cytotoxic activity of NK cells and provide insight into the molecular mechanism of the integration of positive and negative signals during lymphocyte activation.

INTRODUCTION

The initiation and regulation of an immune response are crucially dependent on positive and negative signals that are transmitted by cell surface receptors (*1*). Activating receptors of immune cells include antigen receptors on T and B lymphocytes and stimulatory receptors on natural killer (NK) cells, such as CD16, NKG2D (CD314), NKp30 (CD337), NKp46 (CD335), DNAM-1 (DNAX accessory molecule-1, CD226), and 2B4 (CD244) (*2*). Engagement of NKG2D on NK cells by ligands on tumor cells induces the tyrosine phosphorylation of the associated signaling partner chain DNAX-activating protein of 10 kD (DAP10) by Src family kinases (SFKs) (*3*, *4*). Phosphorylated DAP10 (pDAP10) recruits phosphoinositide 3-kinase (PI3K) and the adaptor protein growth factor receptor–bound protein 2 (Grb2), which results in the recruitment of the guanine nucleotide exchange factor (GEF) Vav1, which is then phosphorylated by SFKs (*5*). Phosphorylated Vav1 (pVav1) triggers a reorganization of the actin cytoskeleton (*6*), which is essential for the clustering of activating receptors, their recruitment into membrane microdomains (*7*, *8*), and the formation of the immunological synapse (IS) (*9*).

The cytotoxic activity of NK cells is inhibited by receptors that recognize major histocompatibility complex type I (MHC-I), such as human killer cell immunoglobulin (Ig)–like receptors (KIRs), mouse inhibitory Ly49 receptors, and the CD94-NKG2A receptor complex, which recognizes the human MHC-I molecule human leukocyte antigen E (HLA-E) (*10*). The activities of these receptors depend on the recruitment of Src homology 2 (SH2) domain–containing protein tyrosine phosphatase 1 (SHP-1) and SHP-2 to phosphorylated immunoreceptor tyrosine-based inhibition motifs (ITIMs) on the receptors. Inhibitory receptors regulate the activities of various activating receptors that couple to diverse signaling pathways. Therefore, the question that arises is whether inhibitory receptors use different mechanisms for different receptor signaling pathways or whether they interfere with a central signaling event that is common to all activating receptors. Vav1 has been identified as a direct target for dephosphorylation by SHP-1 when SHP-1 is recruited to the ITIM of an inhibitory NK cell receptor (*11*, *12*). This may represent the first step at which activating and inhibitory signals converge. By targeting Vav1 for dephosphorylation, inhibitory receptors would effectively interfere with actin reorganization, clustering of activating receptors, and formation of the IS, the contact area between an NK cell and its target, thereby blocking the activation of NK cells at a very early step.

Given the importance of regulating immune cell responses by a balance of positive and negative signals, a better understanding of the integration of these opposing signals at a molecular level would be useful. Here, we used mathematical modeling of the complex interaction of inhibitory and activating signaling pathways in combination with experimental validation of model predictions to understand the nonlinear integration of opposing signals. Biochemical reactions are constrained by the laws of chemical reactions. This enables study of the behavior of complex signal transduction networks by mathematical models based on chemical reaction laws (*13*). However, the results from numerical simulations of these mathematical models are highly dependent on the kinetic parameters that are chosen for model simulations. Here, we investigated the integration logic of positive and negative signals in NK cells, and we present an approach that enables users to generate functional insights into systems even in the case of partially unknown reaction parameters.

RESULTS

Modeling the signal transduction network of NK cells

We constructed a mathematical model that describes the membrane-proximal signaling events that follow the triggering of the activating

[1]Division of Theoretical Bioinformatics, German Cancer Research Center, 69120 Heidelberg, Germany. [2]Institute for Immunology, University of Heidelberg, 69120 Heidelberg, Germany. [3]Institute of Pharmacy and Molecular Biotechnology, BioQuant, University of Heidelberg, 69120 Heidelberg, Germany.
*These authors contributed equally to this work.
†Present address: Freiburg Institute for Advanced Studies and Center for Biosystems Analysis, University of Freiburg, 79104 Freiburg, Germany.
‡To whom correspondence should be addressed. E-mail: r.eils@dkfz.de (R.E.); watzl@uni-hd.de (C.W.)
§Present address: Leibniz Research Center for Working Environment and Human Factors–IfADo, Ardeystrasse 67, 44139 Dortmund, Germany.

receptor NKG2D, the inhibitory receptor CD94-NKG2A, or both (Fig. 1A). The phosphorylation of the signaling molecule Vav1 is the first point at which activating and inhibitory signals might converge; therefore, we used receptor-induced regulation of the phosphorylation of Vav1 as the readout of our model. The model is based on the kinetics of biochemical reactions; that is, we used bimolecular reaction kinetics for associations between molecules, unimolecular reaction kinetics for dissociation reactions, and Michaelis-Menten kinetics for enzymatic reactions (see the Supplementary Materials for more details). Our model assumes that the "cytoplasm," "membrane," and "IS" form three distinct compartments. Although NKG2D (which is symbolized in Fig. 1A by its associated signaling chain DAP10) is localized in the membrane, it makes contact with its ligand MICA [major histocompatibility complex class I (MHC-I) chain–related protein A] only when the receptor is in the IS. Similar to Vav1, the NKG2D-DAP10 complex is tyrosine-phosphorylated by membrane-associated SFKs, which we modeled with a rapidly equilibrating intramolecular conformational change from an open (active) to a closed (autoinhibited) conformation, and vice versa (see the Supplementary Materials). Phosphorylated NKG2D-DAP10 recruits Vav1 through the adaptor molecule Grb2. To simplify the mathematical model, we excluded Grb2 from the system, which is justified for rapidly equilibrating pDAP10-Grb2 and Grb2-Vav1 binding reactions. The inhibitory receptor CD94-NKG2A interacts with its ligand MHC-I in the IS, which results in the phosphorylation of CD94-NKG2A by SFKs and the recruitment of the phosphatase SHP-1. We modeled SHP-1 in a manner similar to that of SFKs as being in either an open or a closed conformation, whereby only the open conformation of the molecule could interact with phosphorylated CD94-NKG2A. The phosphatase CD45 was included in the model and was assumed to dephosphorylate all phosphorylated states if those molecules were accessible, that is, if they were not bound to another protein. The activating and inhibitory receptor signaling cascades communicate through SHP-1–mediated dephosphorylation of Vav1 (*11*).

To address various concepts important to immune receptor signaling, we created a modular library of mechanistically different models, an approach known as ensemble modeling (*14*) (Fig. 1B). The first module, module (a), describes actin reorganization triggered by pVav1 (*6*), which leads to increased recruitment or entrapment of activating receptors in the IS. The second module, module (b), describes the exclusion of the bulky phosphatase CD45 from the IS, as described by the kinetic-segregation hypothesis (*15*). Modules (c) and (g) describe the putative association of SFKs in their open conformation with the phosphorylated activating receptor complex NKG2D-DAP10 (c) or the inhibitory receptor CD94-NKG2A (g) (kinase aggregation). Module (d) describes how SFKs mediate intermolecular autophosphorylation of other SFKs, which results in their enhanced activity (*16*). This can be counteracted by SHP-1–mediated dephosphorylation of SFKs as described by module (e) (*17*). Module (f) assumes that SHP-1 may be phosphorylated by active SFKs to increase its enzymatic activity (*18*). Given the combination of the core model with all of the putative modules, further considering that module (e) requires the presence of module (d), and eliminating the nonphysiological assumption that SFKs associate with inhibitory, but not activating, receptors [module (g) in the absence of (c)], we generated 72 putative models of the proximal signal transduction network of NK cells. (See the Supplementary Materials for the SBML and MATLAB m-files of the model.)

The models were parameterized with kinetic rates that we derived from the published literature (table S1). We performed quantitative Western blotting and flow cytometric analyses to determine the initial concentrations of the intracellular signaling molecules and surface receptors (fig. S1 and table S2). To characterize the input-output behavior of each model for literature-derived kinetic parameters, we computed the steady-state concentration of pVav1 for varying amounts of inhibitory and activating ligands. The 72 different models generated four qualitatively different response behaviors (Fig. 2 and fig. S2). Models that contained only the modules (a), (b), (d), (e), and (f) showed a "valley" response behavior, in which increased amounts of activating and inhibitory ligands decreased the concentration of pVav1 below that found in unstimulated situations (Fig. 2A). Module (c), which assumes the association of SFKs with the activating receptor complex NKG2D-DAP10, changed the behavior of the model; engagement of NKG2D-DAP10 resulted in increased phosphorylation of Vav1, whereas co-engagement of the inhibitory receptor only minimally reduced the extent of phosphorylation of Vav1 (Fig. 2, B and C). Inclusion of module (g), which assumes an association between

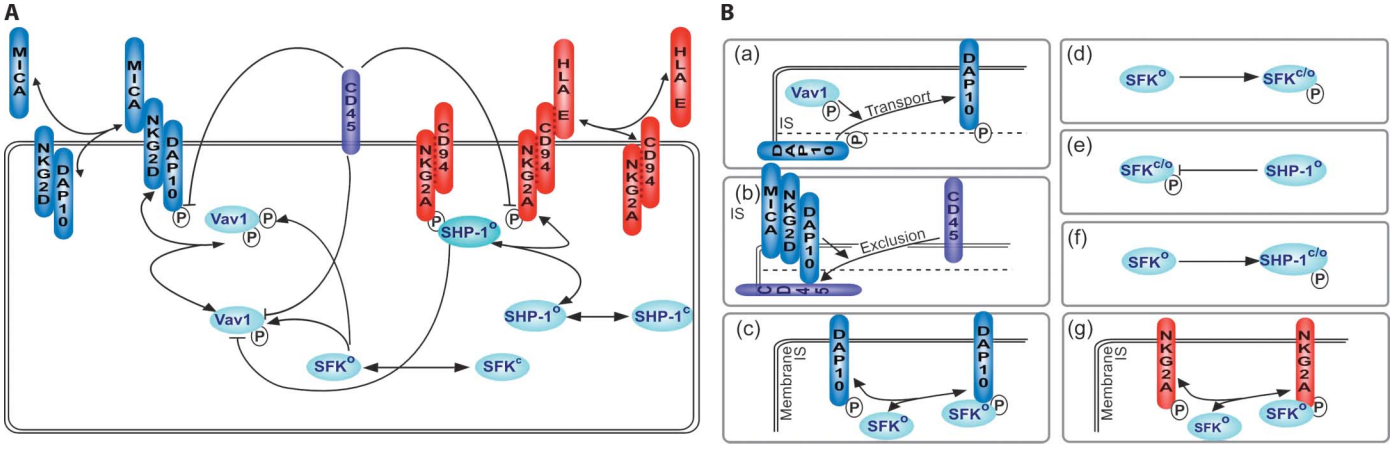

Fig. 1. Modeling the proximal signal transduction network in NK cells. (**A**) Graphical representation of the mathematical core model. Activating receptors and ligands are shown in blue; inhibitory receptors and ligands are shown in red. Unidirectional arrows represent phosphorylation events; bidirectional arrows represent association and dissociation events. Dephosphorylation events are represented by blunt-ended arrows. The three compartments of the model (the IS, cytoplasm, and membrane) are omitted for clarity. (**B**) Optional modules used to expand the core model. The labels (a) through (g) indicate optional modules that can be added to the core model, as described in the Results.

SFKs and the inhibitory receptor CD94-NKG2A, resulted in induction of the phosphorylation of Vav1 upon engagement of activating and inhibitory receptors (Fig. 2D).

Effect of antagonistic signals on Vav1 phosphorylation

To compare the modeling results to the phosphorylation of Vav1 in NK cells, we used the human NK cell line NKL and stimulated the activating receptor NKG2D-DAP10, the inhibitory receptor CD94-NKG2A, or both with different concentrations of specific monoclonal antibodies followed by cross-linking with secondary antibodies to induce receptor clustering. We then determined the extent of Vav1 phosphorylation by quantitative Western blotting analysis (Fig. 3A). Increased engagement of NKG2D-DAP10 stimulated a strong, switch-like induction of Vav1 phosphorylation, which was effectively counteracted by co-engaging CD94-NKG2A. We obtained similar results in experiments with primary NK cells from a donor in which most NK cells expressed the inhibitory receptor KIR2DL2/3 (Fig. 3B). This experimentally observed behavior of Vav1 phosphorylation was different from our initial model predictions but vaguely resembled our simulation results (Fig. 2B), which crucially depended on signaling module (c), which describes the association of a kinase with the activating receptor.

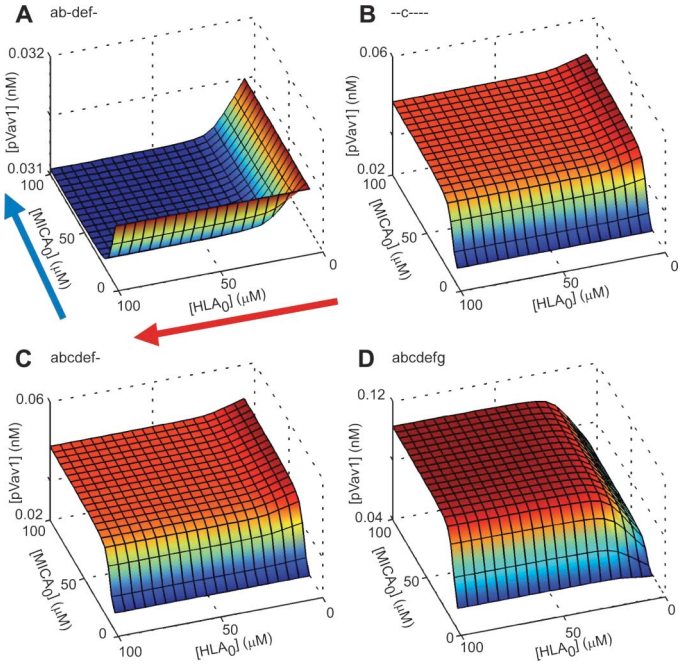

Fig. 2. Dose-response profiles of pVav1 for different model variants. With kinetic parameters derived from the literature (tables S1 and S4), we calculated the steady-state phosphorylation of Vav1 (*z* axis, pVav1) after target cell contact for different concentrations of activating ligand (blue arrow, *y* axis, $MICA_0$) and inhibitory ligand (red arrow, *x* axis, HLA_0), which are plotted in reverse for better visibility of the results. The ligand concentrations used as an input to the models refer to the concentrations in the target cell subcompartment directly in contact with the NK cell. The letter codes above each panel indicate the modules that were included in the model. (**A**) Example for models without module (c). (**B** and **C**) Examples for models with module (c). (**D**) Example for a model additionally including module (g). For better visibility, the amount of pVav1 is plotted with a heat map ranging from low (blue) to high (red) concentrations. The results for all 72 models are shown in fig. S2.

Essential role of kinase association with activating receptors

The behaviors of in silico models are highly dependent on the kinetic rate values; however, the respective parameter values that we extracted from the literature (table S1) varied more than two orders of magnitude, and the experimental methods that were used for the measurement of these rates differed markedly from the situation in vivo. To reduce the dependence of our results on poorly identified parameter values, we conducted an extended exploration of the parameter space. We drew the kinetic rates of all of the reactions from a logarithmic uniform distribution that extended four orders of magnitude around the geometric mean of the literature-derived parameters (table S4), and we then computed the steady-state response of each model. For each model, we tested 5000 different parameter sets. The resulting 360,000 dose-response profiles were

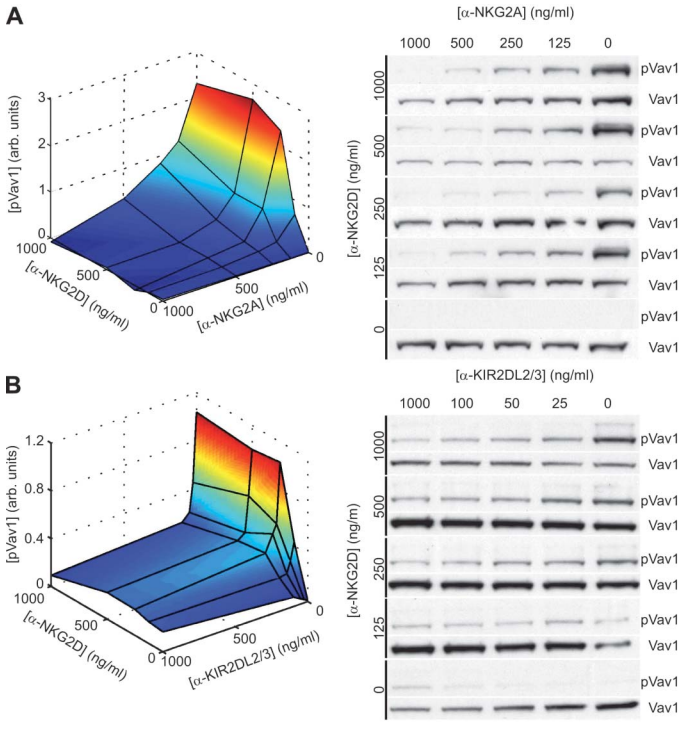

Fig. 3. Phosphorylation of Vav1 in NK cells in response to the triggering of activating and inhibitory receptors. (**A**) NKL cells were incubated with the indicated concentrations of mouse antibodies against the activating receptor complex NKG2D-DAP10 (α-NKG2D) and the inhibitory receptor complex CD94-NKG2A (α-NKG2A). After cross-linking with secondary goat antibodies against the primary mouse antibodies, the cells were incubated at 37°C for 5 min. The extent of Vav1 phosphorylation (amount of pVav1 protein) was determined by Western blotting analysis of cell lysates with an antibody specific for pVav1, followed by an antibody against total Vav1 as a loading control. Blots were analyzed by densitometric scanning, and the extent of Vav1 phosphorylation was calculated by dividing the signal for pVav by that for total Vav. A graphical representation of the results is shown on the left using the same heat map for pVav1 as described for Fig. 2. Data are representative of three independent experiments. arb., arbitrary. (**B**) NKG2D-mediated phosphorylation of Vav1 was determined as described in (A) with primary human NK cells from one donor in which more than 85% of the NK cells expressed the inhibitory receptor KIR2DL2/3.

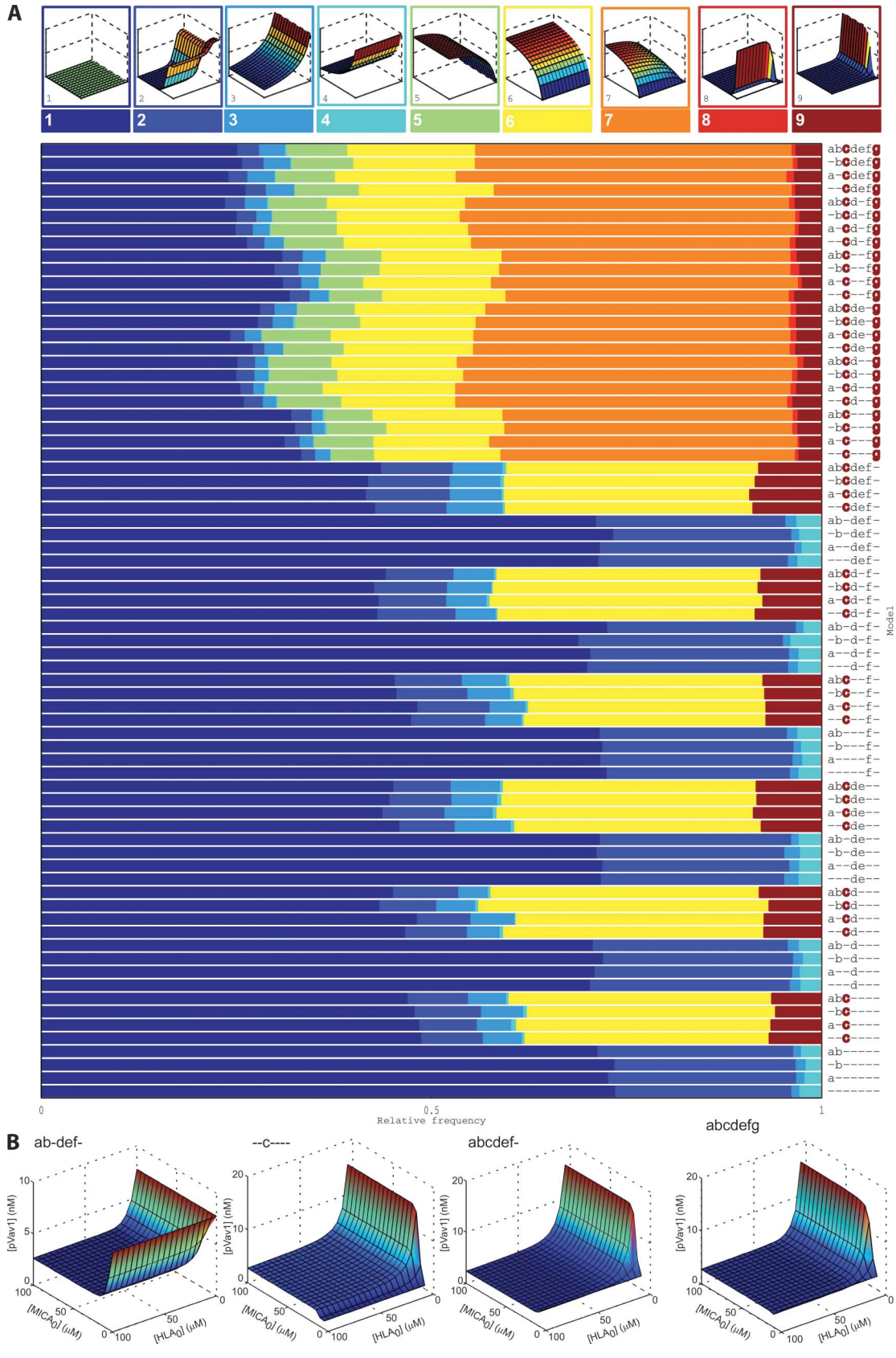

Fig. 4. Testing the parameter dependency of the model. (**A**) Parameter scan: The kinetic parameters for all 72 different models (the module codes are indicated on the right) were randomly varied over four orders of magnitude around the geometric means of the literature-derived parameters. For each model, 5000 different parameter sets were tested. The steady-state pVav1 response of each model was computed and compared to the nine different response curves shown on top. The classification of the 5000 results for each model is shown as the relative frequency of each response curve with the color code indicated for the nine different response curves on top. (**B**) Parameter fit: Starting with a parameter set from (A) that generated a pVav dose-response profile with the minimal least-squares residual with respect to the experimental data (Fig. 3), we fit the kinetic parameters of the indicated models to the experimental pVav1 dose-response behavior (see table S4 for fitted parameters). Data are plotted as described for Fig. 2. Models without module (c) (left panel) were not able to generate a physiologic pVav1 output, whereas any model containing module (c) could be fitted to produce a physiologic pVav1 output.

classified into nine different "response shapes" (Fig. 4A and table S3). Testing for a larger number of parameter combinations did not change the results qualitatively. The basic core model was not able to produce a physiologic Vav1 phosphorylation output (represented by the dark red region of shape 9) with any of the 5000 random parameter sets (Fig. 4A). Similarly, adding the module (a) (actin reorganization), (b) (kinase-phosphatase segregation), (d) (kinase autophosphorylation), (e) (SHP-1–mediated dephosphorylation of autophosphorylated kinases), or (f) (phosphorylation fo SHP-1) to the model either alone or in combination did not improve the results. Only those models that contained module (c), which describes the association of an SFK with the activating receptor, produced a physiologic Vav1 response for up to 9% of the random parameter sets. About 30% of the parameter sets in models that contained module (c) produced a response (Fig. 4A, shape 6, yellow) in which engagement of the activating receptor increased the extent of Vav1 phosphorylation, but co-engagement of the inhibitory receptor did not alter this response. When we analyzed the differences between the parameter sets that created such a response and the parameter sets that created a physiologic Vav1 phosphorylation response, we found that parameters that favored the phosphorylation of the inhibitory receptor CD94-NKG2A, the binding of SHP-1 to CD94-NKG2A, and the dephosphorylation of Vav1 by SHP-1 were required to enable CD94-NKG2A–mediated inhibition of Vav1 phosphorylation (fig. S3A).

When we combined module (g) (association of an SFK with the inhibitory receptor) with models containing module (c), we found that fewer parameter sets could recreate a physiological Vav1 response, and about 40% of the random parameters created a response in which engagement of activating and inhibitory receptors resulted in increased Vav1 phosphorylation (Fig. 4A, shape 7). This suggested that the association of SFKs with inhibitory receptors converted them into activating receptors. When we analyzed the differences between the parameter sets that generated this response and the parameters that generated a physiologic Vav1 phosphorylation response, we found that parameters that favored the association of SHP-1, but not SFKs, with CD94-NKG2A and the increased dephosphorylation of Vav1 by SHP-1 were required to transform CD94-NKG2A from an activating receptor into an inhibitory one (fig. S3B).

To further investigate the role of the association of SFKs with activating receptors for the creation of a physiologic pVav1 response, we performed a parameter fit. In this approach, we fit the kinetic parameters of each model to the experimental data (fig. S4 and table S4). We started with a parameter set from the parameter scan that generated a pVav dose-response profile with the minimal least-squares residual with respect to the experimental data (Fig. 3). With this approach, the core model showed a local increase in the abundance of pVav in the IS compartment, which was induced by stimulation of the activating receptor. However, this increase in amount of pVav in the IS was accompanied by an equivalent decrease in the amounts of pVav in the membrane and cytoplasmic compartments. Thus, in contrast to our experimental data, no increase in the total amount of pVav was induced. Similarly, other models lacking module (c) failed to approximate the experimental results (Fig. 4B); however, inclusion of module (c) was sufficient to create a physiologic Vav1 response. These data show that our model, which incorporated only the very early events after the engagement of NKG2D-DAP10, CD94-NKG2A, or both, could accurately predict a physiological Vav1 phosphorylation response, and they demonstrate an essential role for the association of SFKs with the activating receptor.

Quantification of the extent of Vav1 phosphorylation

To quantify the number of phosphorylation events, we stimulated NK cells through the engagement of the activating receptor NKG2D-DAP10 or the inhibitory complex CD94-NKG2A and determined the extent of phosphorylation of SFKs and Vav1. To obtain quantitative data, we used cells pretreated with either the SFK inhibitor PP1, to establish the minimal extent of phosphorylation, or pervanadate, which induced maximal phosphorylation (fig. S5). Maximal engagement of NKG2D-DAP10 by antibody-mediated cross-linking increased the amount of pVav1 from 0.4% of the total Vav1 to ~11% (Fig. 5A); however, this stimulation failed to induce substantial phosphorylation of SFKs. Engagement of the inhibitory CD94-NKG2A complex did not result in substantial changes in the extent of phosphorylation of Vav1 or SFKs. These results confirmed that SFK autophosphorylation, as described by module (d), did not play a substantial role in our experimental system. The data further showed that engagement of NKG2D-DAP10 resulted in concentrations of pVav1 in NK cells of up to 19 nM. Similar concentrations of pVav1 (~16 nM) were predicted in our modeling approach (Fig. 4B), demonstrating the reliability of our model.

Stimulation-dependent association of SFKs with NKG2D-DAP10

To experimentally test for the association of SFKs with phosphorylated activating receptors, we stimulated NKG2D-DAP10 by antibody-mediated cross-linking, lysed the cells in the mild detergent Brij-58, and isolated the stimulated receptors with magnetic beads (Fig. 5B). We observed an association of Vav1 and the SFKs Lck and Fyn specifically with the stimulated NKG2D receptor. The extent of the associations of Lck and Fyn with stimulated NKG2D represented increases, relative to their association with the unstimulated receptor, by factors of ~11 and ~44, respectively (Fig. 5B). Engagement of NKG2D also induced the phosphorylation of Vav1, which was detectable at the receptor and in cell lysates. Notably, the ratio of the amount of pVav1 to that of total Vav1 was about 30 times higher in association with NKG2D than in the lysate (Fig. 5B), which suggests that activated NKG2D-DAP10 triggered the phosphorylation of Vav1. These data confirm the activation-dependent association between NKG2D-DAP10 and Fyn and Lck, as suggested by the essential role of module (c) (kinase association) in our model.

Kinetics of Vav1 phosphorylation

To further test our model with the fitted parameters (Fig. 4B), we used the core model containing module (c) and calculated the kinetic change in Vav1 phosphorylation upon triggering of NKG2D-DAP10. This calculation predicted a rapid increase in extent of Vav1 phosphorylation, which reached a plateau after ~250 s (Fig. 5C). Although lowering the initial concentration of MICA reduced the amplitude of Vav1 phosphorylation, the time needed to reach the plateau remained unchanged. To validate these results experimentally, we stimulated NKG2D-DAP10 on NK cells and determined the kinetics of Vav1 phosphorylation. In agreement with the simulation, we observed a rapid increase in Vav1 phosphorylation, which reached its maximum after ~200 to 300 s. Reduced engagement of NKG2D resulted in a lower amount of pVav1 with unchanged kinetics, consistent with the predictions from our model. We also observed a reduction in Vav1 phosphorylation between 5 and 10 min after receptor engagement, which suggested the presence of inhibitory signaling pathways that were not incorporated in our model.

A model simulation with decreased SFK activity predicted a delayed increase in Vav1 phosphorylation and a decrease in the final concentration of pVav1 (Fig. 5D). To test these predictions experimentally, we measured the phosphorylation of Vav1 in response to engaging NKG2D-DAP10 in the presence of the SFK inhibitor PP1. In agreement with the predictions, increasing the concentration of PP1 affected the

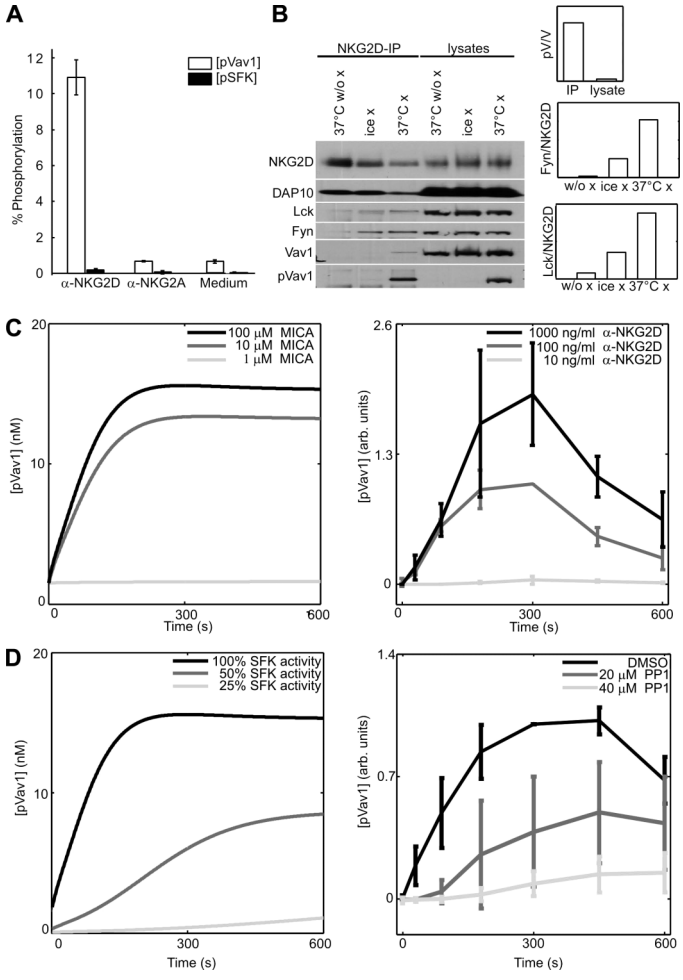

Fig. 5. Association of SFKs with NKG2D and kinetic analysis of the model. (A) The amounts of pVav1 and phosphorylated SFK (pSFK) were determined by quantitative Western blotting analysis, as described for Fig. 3. Through the use of cells treated with PP1 (negative control) or pervanadate (positive control) as standards (Supplementary Materials and fig. S5), we calculated the relative amounts of pVav1 and the indicated pSFKs relative to those of total Vav1 and SFK. Data represent the mean of three experiments. (B) NKL cells were treated with antibodies against NKG2D and incubated at 37°C for 5 min (37°C w/o x) or were additionally incubated with goat anti-mouse antibodies on ice (ice x) or at 37°C for 5 min (37°C x). Cells were then lysed and NKG2D was immunoprecipitated. Immunoprecipitated samples (NKG2D-IP, shown in the blot on the left) and lysates from the samples before immunoprecipitation (as loading controls) were analyzed by Western blotting with the indicated antibodies. Cross-linking of NKG2D at 37°C resulted in a slightly reduced recovery of the receptor complex from the lysate. The ratio between the signal for pVav1 corrected for total Vav1 (pV/V) was quantified for the immunoprecipitation of the stimulated NKG2D receptor (IP) and the stimulated lysate (top right panel). The ratios between the amounts of Fyn and NKG2D (middle right panel) and those of Lck and NKG2D (bottom right panel) were quantified for the immunoprecipitated NKG2D samples. Data are representative of at least three experiments. (C) Kinetic changes in Vav1 phosphorylation depending on differential engagement of the activating receptor. The indicated concentrations of the NKG2D ligand MICA were used in the model to calculate the kinetic change in Vav1 phosphorylation (left panel). The extent of Vav1 phosphorylation was then determined experimentally by cross-linking NKG2D on NKL cells with the indicated concentrations of antibodies against NKG2D (right panels), as described for Fig. 3. Means and SDs from three experiments are shown. (D) Kinetic changes in Vav1 phosphorylation depending on SFK activity. The activities of SFKs were reduced to 50 or 25% of their original activities of the model, and the kinetic changes in Vav1 phosphorylation were calculated (left panel). The extent of Vav1 phosphorylation was then determined experimentally by antibody-mediated (1 μg/ml) cross-linking of NKG2D on NKL cells pretreated for 30 min with the indicated concentrations of PP1 (right panels). Means and SDs from three independent experiments are shown.

kinetics, slope, and amplitude of Vav1 phosphorylation. PP1 also reduced the extent of Vav1 phosphorylation after 5 min of combined engagement of NKG2D-DAP10 and NKG2A-CD94 while preserving the overall shape of the response, which was also consistent with the predictions of our model (fig. S6).

Correlation between pVav1 and NK cell cytotoxicity

Our hypothesis was based on the assumption that the signals from activating and inhibitory receptors were integrated at the level of Vav1 phosphorylation. If this were the decision-making point for NK cell activation, then the extent of Vav1 phosphorylation should correlate with the cytotoxic activity of the NK cell. We therefore determined the cytotoxic activity of NK cells upon differential triggering of activating and inhibitory receptors. We found that increasing the extent of NKG2D-DAP10 engagement on NKL cells resulted in a rapid increase in NK cell cytotoxicity, which quickly reached a plateau (Fig. 6A). Co-engagement of the inhibitory CD94-NKG2A receptor effectively blocked NK cell cytotoxicity. We observed a similar dose response in experiments with an NK cell clone expanded from primary human NK cells (Fig. 6B). This cytotoxic response of NK cells paralleled the extent of Vav1 phosphorylation that was predicted by our mathematical model (Fig. 6C), supporting the hypothesis that the amount of pVav1 establishes a key checkpoint for NK cell cytotoxic activity.

DISCUSSION

Effective immune responses are regulated by positive and negative signals; it is therefore important to be able to understand the integration of these opposing signals at a molecular level. Here, we characterized the NK cell signal transduction network upstream of Vav1 and identified key elements of this network through an ensemble modeling approach. Although we used NKG2D-DAP10 and CD94-NKG2A in our model and experimental verifications, our results are likely applicable to other activating and inhibitory NK receptors as well. In addition, the initial kinetic parameters for the association of SFKs with the YINM motif of DAP10 were derived from the known association of SFKs with the immunoreceptor tyrosine-based activation motifs (ITAMs) of T cell receptors (TCRs). Thus, our model may also be applicable to the stimulation of NK cells through ITAM-based receptors, such as CD16, NKp30, NKp44, and NKp46. Because of the large quantity of cells needed for biochemical analysis, we used the human NK cell line NKL in many experiments; however, our model gave similar results with the spatial

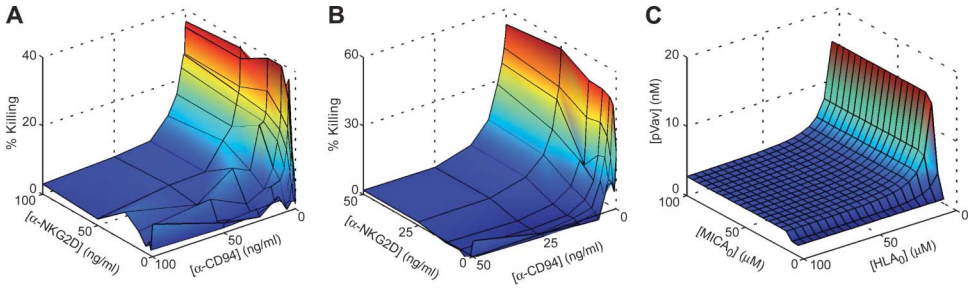

Fig. 6. The cytotoxic activity of NK cells correlates with the extent of Vav1 phosphorylation. (**A** and **B**) NKL cells (A) and a primary human NK cell clone (B) expressing the inhibitory receptor CD94-NKG2A were used in a 4-hour redirected ^{51}Cr-release assay using the Fc receptor–expressing cell line P815 as a target. NKG2D and CD94 were triggered with the indicated concentrations of specific monoclonal antibodies; the resulting lysis of the target cells is indicated as the percent killing. Data are representative of five (A) and two (B) independent experiments. (**C**) Calculated pVav1 response upon differentially triggering activating and inhibitory receptors with model –c—.

dimensions and concentrations of signaling molecules of NKL cells and primary human NK cells. In addition, the functional responses of these cells to the triggering of inhibitory and activating receptors were comparable (Figs. 3B and 6). Thus, our findings will likely be of general relevance to the regulation of human NK cells.

Our data showed that we could obtain a physiologic output of our base model including just the module that described the association of kinases with activating receptors [module (c)]. Whereas this finding demonstrates that this process was essential for the regulation of NK cells, it does not exclude the possibility that the remaining optional modules may play a role during the fine-tuning of NK cell responses. Kinase-phosphatase segregation [module (b)] has been suggested as a mechanism for the initiation of TCR signaling (*15*). CD45 is not necessary for NK cell cytotoxicity (*19*–*21*), consistent with the dispensable role of module (b) in our model. In the case of module (d), which described the autophosphorylation of SFKs, we experimentally excluded the possibility of SFK phosphorylation after NK cell activation, a finding that is consistent with the lack of phosphorylation of SFKs upon T cell activation (*22*). Similarly, we did not detect any phosphorylation of SHP-1 after triggering activating and inhibitory receptors either alone or in combination, which argues against an involvement of SHP-1 phosphorylation, as described by module (f), during NK cell regulation. The stabilization of the active conformation of SHP-1 by ITIM binding as implemented in our model would create a locally high concentration of active SHP-1 at the site of engaged inhibitory receptors. Similarly, the clustering of activating receptors at the IS creates a locally high concentration of active SFKs. This may explain the switch-like regulation of Vav1 phosphorylation and potentially provides the basis for the local regulation of NK cell activity (*23*), in which inhibitory receptors block the activation of NK cells only when co-engaged with activating receptors. Only a fraction of the total Vav1 (~11%) was phosphorylated after the triggering of NKG2D, which could be explained by the fact that the local phosphorylation of Vav1 induced by contact with target cells was sufficient for the full activation of NK cells.

Our data showed a reduction in the extent of Vav1 phosphorylation, which started about 5 min after triggering of NKG2D-DAP10, suggesting the existence of inhibitory feedback loops. This negative feedback was not predicted by our model, because our simulation showed only a slight reduction in the extent of Vav1 phosphorylation at later time points (Fig. 5). The inclusion of any of the optional modules also did not recreate this reduction in Vav1 phosphorylation. Therefore, although we cannot identify the nature of this inhibitory element, we can exclude that any of our optional modules were sufficient for this response. It will be important to identify this inhibitory element in future experiments, because this may be one of the mechanisms that enable serial killing by NK cells (*24*).

We confirmed the association of SFKs with the activating NKG2D-DAP10 receptor in our experiments. These data might be explained by a direct association between SFKs and NKG2D-DAP10, similar to the interaction between Lck and the YxxM motif of CD227 in T cells (*25*); however, engagement of NKG2D-DAP10 results in the recruitment of the receptor complex to specialized membrane microdomains (*7*) at which SFKs are enriched (*26*). The association between NKG2D-DAP10 and SFKs may therefore also arise from the colocalization of these molecules in the same membrane domain. We have made similar observations for the activating receptor 2B4 (*8*), and a report has shown that the confinement of activating receptors to membrane microdomains is correlated with the functional competence of NK cells (*27*). This suggests that the close proximity between activating receptors and SFKs might be essential for NK cell activation. The resulting increased local concentration of SFKs around activating receptors may be one way of transmitting a stimulus across the plasma membrane. Our model shows that this mechanism is sufficient to induce NK cell activation without the need for conformational changes in the receptor, kinase autophosphorylation, or the exclusion of phosphatases (*15*).

Module (g) assumes an association between SFKs and the phosphorylated inhibitory receptor. This was the only module that reduced the number of random parameter sets in our parameter scan that produced a physiological output. Therefore, the association of SFKs with inhibitory receptors may not be compatible with the inhibitory function of these receptors. This was confirmed by the fact that only parameters that favored association of SHP-1 with CD94 rather than association of SFKs with CD94 were compatible with a physiologic Vav1 phosphorylation response. We previously showed that inhibitory receptors do not associate with membrane microdomains (*8*), making colocalization of inhibitory receptors and SFKs within the same membrane domain unlikely. These data suggest that an association between inhibitory receptors and SFKs may not be necessary for the regulation of NK cell activity. The association of SFKs with inhibitory receptors could transform these receptors into activating receptors whose engagement would promote Vav1 phosphorylation (Fig. 4A). During the development of NK cells, inhibitory receptors play an important role in creating functionally competent NK cells (*28*). It is thought that during this process, inhibitory receptors may transmit a positive signal (*29*). Our data may provide a solution to this contradiction by demonstrating that simple changes in the signaling environment can transform an inhibitory receptor into a stimulating receptor.

Our model is based on the finding that Vav1 is a direct substrate of SHP-1 when SHP-1 is bound to an inhibitory receptor (*11*). Peterson and Long showed that c-Cbl can associate with Vav1 that is targeted for dephosphorylation by SHP-1 (*12*). Additionally, the adaptor protein Crk is phosphorylated during inhibitory signaling, which prevents the formation of a complex among c-Cbl, Crk, and the guanidine exchange factor C3G (*12*). Although our data show that we can obtain a physiologic NK cell response in our mathematical model without considering the phosphorylation

of Crk, this does not exclude the existence of such additional regulatory pathways, which may be important for additional fine-tuning of this system.

Our data show a switch-like regulation of Vav1 phosphorylation, which was rapidly induced to maximal extent upon small changes in the engagement of activating receptors. Similarly, small changes in inhibitory receptor signaling were sufficient to almost completely abolish the phosphorylation of Vav1. This behavior correlated with the cytotoxic activity of NK cells. Therefore, we suggest that Vav1 phosphorylation is a key checkpoint in NK cell activation and represents a necessary and essential part of the decision-making system that integrates signals from activating and inhibitory receptors to determine the activity of an NK cell. Although NK cells are exclusively regulated through the balance of positive and negative signals, it is interesting to speculate that Vav1 might also play a role in the interplay between activating and inhibitory receptors in other immune cells.

MATERIALS AND METHODS

Reagents, cells, and antibodies

The murine mastocytoma cell line P815, the human NK cell line NKL, and primary human NK cells and clones were purified and cultured as previously described (*30*, *31*). Antibodies used in this study included control mouse IgG1 (MOPC21, Sigma), goat antibodies against mouse IgG (Dianova), horseradish peroxidase (HRP)–conjugated goat antibody against rabbit IgG (Santa Cruz Biotechnology), and antibodies against the following targets: NKG2D (149810, R&D Systems); NKG2A-CD159a (Z199), CD94 (HP-3B1), KIR2DL1 (EB6), and KIR2DL2/3 (GL183) (all from Beckman Coulter); pVav1 (pY^{160}, Biosource); Vav (VAV-30, Abcam and Upstate); SHP-1 (BD Transduction Laboratories); Lck (a rabbit polyclonal antibody that was a gift of A. Veillette, University of Montreal, Canada); and Fyn (rabbit antibody), pSrc family (Tyr^{416}), and total, nonphosphorylated Src (7G9) (Tyr^{416}) (all from Cell Signaling Technology).

Redirected lysis assay

Standard ^{51}Cr-release assays were performed as previously described (*32*). Effector and P815 target cells were mixed at a constant ratio with the indicated antibody concentrations. In some experiments, effector cells were preincubated for 30 min at 37°C with PP1 (Biomol) or dimethyl sulfoxide (DMSO) as a control.

Receptor cross-linking, immunoprecipitations, and Western blotting analysis

Cells were resuspended at 2×10^7/ml in Iscove's modified Dulbecco's medium containing 10% fetal calf serum and 1% penicillin and streptomycin and, in some experiments, were preincubated for 30 min at 37°C with various concentrations of PP1 or DMSO. Cells were incubated with primary antibodies for 10 min at room temperature. Cells were washed and then incubated with goat antibody against mouse IgG (5 μg/ml) for 5 min at 37°C. Stimulation was stopped by immediately adding ice-cold medium and putting the cells on ice. Lysis and Western blotting analysis were performed as previously described (*8*). For immunoprecipitations, cells were lysed in a buffer containing 1% Brij-58 (AppliChem) and DNase I (deoxyribonuclease I, 200 Kunitz units/ml, Sigma). Lysates of 1×10^7 cells per sample were incubated with antibody against mouse IgG (5 μg/ml) with gentle agitation for 20 min, after which Protein G Dynabeads (12.5 μl, Invitrogen) were added for 2 hours at 4°C. Beads were washed five times with lysis buffer, and proteins were eluted with 50 mM glycine (pH 2.0) and then used for Western blotting analysis. Western blots were quantified with a densitometer (Bio-Rad GS800) and Quantity One software.

Mathematical modeling and analysis

The complete mathematical model representing all of the model variants was formulated with SBML (Systems Biology Markup Language)–shorthand (http://www.staff.ncl.ac.uk/d.j.wilkinson) and translated by the accompanying python script into the SBML (http://www.sbml.org). The 72 alternative models were generated from the complete model by adapting the parameters accordingly. All subsequent simulations and analyses were computed with the MATLAB (MathWorks) programming language; the open-source MATLAB toolboxes SBMLToolbox (*33*), SBToolbox (*34*), and SBaddon (*35*); and in-house algorithms (which are available upon request). All computations were started from the unstimulated steady state. Dose-response curves were computed by linearly varying ligand concentrations and simulating the model until a new steady state was reached. Kinetic parameters were fitted with the lsqnonlin function from the MATLAB Optimization Toolbox. To scan and classify the parameter space, we computed the dose-response profile of each model 5000 times with random values chosen from 0.01 to 100 times the geometric mean of the literature values. By numerically preselecting and visually inspecting 4800 dose-response profiles, we qualitatively classified the profiles into nine different shapes (table S3). Analytical functions describing these nine shapes were defined and fitted with the MATLAB lsqnonlin function to the 360,000 dose-response profiles to provide the minimal least-squares residual.

SUPPLEMENTARY MATERIALS

www.sciencesignaling.org/cgi/content/full/4/175/ra36/DC1

Methods

Fig. S1. Quantification of cytosolic proteins by Western blotting analysis.

Fig. S2. Initial simulation results.

Fig. S3. Interclass parameter ratios.

Fig. S4. Results of the parameter fit for all 72 models.

Fig. S5. Quantification of the total amounts of pVav1 and pSFK after stimulation of NK cells.

Fig. S6. Comparison between predicted and experimentally observed pVav1 responses after treatment with PP1.

Table S1. Kinetic parameters used for modeling.

Table S2. Protein numbers and concentrations for different NK cell types.

Table S3. Table of shape functions and their analytical equations used for the classification of shapes generated in the parameter scan.

Table S4. Literature-derived and fitted kinetic rates.

References

MATLAB and SBML model files.

REFERENCES AND NOTES

1. D. D. Billadeau, P. J. Leibson, ITAMs versus ITIMs: Striking a balance during cell regulation. *J. Clin. Invest.* **109**, 161–168 (2002).
2. L. L. Lanier, NK cell recognition. *Annu. Rev. Immunol.* **23**, 225–274 (2005).
3. D. D. Billadeau, J. L. Upshaw, R. A. Schoon, C. J. Dick, P. J. Leibson, NKG2D-DAP10 triggers human NK cell–mediated killing via a Syk-independent regulatory pathway. *Nat. Immunol.* **4**, 557–564 (2003).
4. L. L. Lanier, Up on the tightrope: Natural killer cell activation and inhibition. *Nat. Immunol.* **9**, 495–502 (2008).
5. J. L. Upshaw, L. N. Arneson, R. A. Schoon, C. J. Dick, D. D. Billadeau, P. J. Leibson, NKG2D-mediated signaling requires a DAP10-bound Grb2-Vav1 intermediate and phosphatidylinositol-3-kinase in human natural killer cells. *Nat. Immunol.* **7**, 524–532 (2006).
6. D. B. Graham, M. Cella, E. Giurisato, K. Fujikawa, A. V. Miletic, T. Kloeppel, K. Brim, T. Takai, A. S. Shaw, M. Colonna, W. Swat, Vav1 controls DAP10-mediated natural cytotoxicity by regulating actin and microtubule dynamics. *J. Immunol.* **177**, 2349–2355 (2006).
7. J. Endt, F. E. McCann, C. R. Almeida, D. Urlaub, R. Leung, D. Pende, D. M. Davis, C. Watzl, Inhibitory receptor signals suppress ligation-induced recruitment of NKG2D to GM1-rich membrane domains at the human NK cell immune synapse. *J. Immunol.* **178**, 5606–5611 (2007).

8. C. Watzl, E. O. Long, Natural killer cell inhibitory receptors block actin cytoskeleton-dependent recruitment of 2B4 (CD244) to lipid rafts. *J. Exp. Med.* **197**, 77–85 (2003).
9. J. S. Orange, Formation and function of the lytic NK-cell immunological synapse. *Nat. Rev. Immunol.* **8**, 713–725 (2008).
10. E. O. Long, Negative signaling by inhibitory receptors: The NK cell paradigm. *Immunol. Rev.* **224**, 70–84 (2008).
11. C. C. Stebbins, C. Watzl, D. D. Billadeau, P. J. Leibson, D. N. Burshtyn, E. O. Long, Vav1 dephosphorylation by the tyrosine phosphatase SHP-1 as a mechanism for inhibition of cellular cytotoxicity. *Mol. Cell. Biol.* **23**, 6291–6299 (2003).
12. M. E. Peterson, E. O. Long, Inhibitory receptor signaling via tyrosine phosphorylation of the adaptor Crk. *Immunity* **29**, 578–588 (2008).
13. B. B. Aldridge, J. M. Burke, D. A. Lauffenburger, P. K. Sorger, Physicochemical modelling of cell signalling pathways. *Nat. Cell Biol.* **8**, 1195–1203 (2006).
14. L. Kuepfer, M. Peter, U. Sauer, J. Stelling, Ensemble modeling for analysis of cell signaling dynamics. *Nat. Biotechnol.* **25**, 1001–1006 (2007).
15. S. J. Davis, P. A. van der Merwe, The kinetic-segregation model: TCR triggering and beyond. *Nat. Immunol.* **7**, 803–809 (2006).
16. J. A. Cooper, A. MacAuley, Potential positive and negative autoregulation of p60c-src by intermolecular autophosphorylation. *Proc. Natl. Acad. Sci. U.S.A.* **85**, 4232–4236 (1988).
17. G. G. Chiang, B. M. Sefton, Specific dephosphorylation of the Lck tyrosine protein kinase at Tyr-394 by the SHP-1 protein-tyrosine phosphatase. *J. Biol. Chem.* **276**, 23173–23178 (2001).
18. W. Lu, D. Gong, D. Bar-Sagi, P. A. Cole, Site-specific incorporation of a phosphotyrosine mimetic reveals a role for tyrosine phosphorylation of SHP-2 in cell signaling. *Mol. Cell* **8**, 759–769 (2001).
19. D. G. Hesslein, R. Takaki, M. L. Hermiston, A. Weiss, L. L. Lanier, Dysregulation of signaling pathways in CD45-deficient NK cells leads to differentially regulated cytotoxicity and cytokine production. *Proc. Natl. Acad. Sci. U.S.A.* **103**, 7012–7017 (2006).
20. N. D. Huntington, Y. Xu, S. L. Nutt, D. M. Tarlinton, A requirement for CD45 distinguishes Ly49D-mediated cytokine and chemokine production from killing in primary natural killer cells. *J. Exp. Med.* **201**, 1421–1433 (2005).
21. L. H. Mason, J. Willette-Brown, L. S. Taylor, D. W. McVicar, Regulation of Ly49D/DAP12 signal transduction by Src-family kinases and CD45. *J. Immunol.* **176**, 6615–6623 (2006).
22. W. Paster, C. Paar, P. Eckerstorfer, A. Jakober, K. Drbal, G. J. Schütz, A. Sonnleitner, H. Stockinger, Genetically encoded Förster resonance energy transfer sensors for the conformation of the Src family kinase Lck. *J. Immunol.* **182**, 2160–2167 (2009).
23. M. Eriksson, G. Leitz, E. Fällman, O. Axner, J. C. Ryan, M. C. Nakamura, C. L. Sentman, Inhibitory receptors alter natural killer cell interactions with target cells yet allow simultaneous killing of susceptible targets. *J. Exp. Med.* **190**, 1005–1012 (1999).
24. R. Bhat, C. Watzl, Serial killing of tumor cells by human natural killer cells—enhancement by therapeutic antibodies. *PLoS One* **2**, e326 (2007).
25. P. Mukherjee, T. L. Tinder, G. D. Basu, S. J. Gendler, MUC1 (CD227) interacts with lck tyrosine kinase in Jurkat lymphoma cells and normal T cells. *J. Leukoc. Biol.* **77**, 90–99 (2005).
26. A. M. Shenoy-Scaria, L. K. Gauen, J. Kwong, A. S. Shaw, D. M. Lublin, Palmitylation of an amino-terminal cysteine motif of protein tyrosine kinases $p56^{lck}$ and $p59^{fyn}$ mediates interaction with glycosyl-phosphatidylinositol-anchored proteins. *Mol. Cell. Biol.* **13**, 6385–6392 (1993).
27. S. Guia, B. N. Jaeger, S. Piatek, S. Mailfert, T. Trombik, A. Fenis, N. Chevrier, T. Walzer, Y. M. Kerdiles, D. Marguet, E. Vivier, S. Ugolini, Confinement of activating receptors at the plasma membrane controls natural killer cell tolerance. *Sci. Signal.* **4**, ra21 (2011).
28. N. T. Joncker, D. H. Raulet, Regulation of NK cell responsiveness to achieve self-tolerance and maximal responses to diseased target cells. *Immunol. Rev.* **224**, 85–97 (2008).
29. W. M. Yokoyama, S. Kim, How do natural killer cells find self to achieve tolerance? *Immunity* **24**, 249–257 (2006).
30. P. Eissmann, C. Watzl, Molecular analysis of NTB-A signaling: A role for EAT-2 in NTB-A-mediated activation of human NK cells. *J. Immunol.* **177**, 3170–3177 (2006).
31. M. M. Sandusky, B. Messmer, C. Watzl, Regulation of 2B4 (CD244)-mediated NK cell activation by ligand-induced receptor modulation. *Eur. J. Immunol.* **36**, 3268–3276 (2006).
32. B. Messmer, P. Eissmann, S. Stark, C. Watzl, CD48 stimulation by 2B4 (CD244)-expressing targets activates human NK cells. *J. Immunol.* **176**, 4646–4650 (2006).
33. S. M. Keating, B. J. Bornstein, A. Finney, M. Hucka, SBMLToolbox: An SBML toolbox for MATLAB users. *Bioinformatics* **22**, 1275–1277 (2006).
34. H. Schmidt, M. Jirstrand, Systems Biology Toolbox for MATLAB: A computational platform for research in systems biology. *Bioinformatics* **22**, 514–515 (2006).
35. H. Schmidt, SBaddon: High performance simulation for the Systems Biology Toolbox for MATLAB. *Bioinformatics* **23**, 646–647 (2007).

36. **Acknowledgments:** We thank B. Messmer, S. Wingert, and I. Cado for experimental support; Y. Samstag and A. Veillette for sharing reagents; and E. Long for critical reading of the manuscript. **Funding:** This work was supported by the Initiative and Networking Fund of the Helmholtz Association within the Helmholtz Alliance on Systems Biology/SBCancer by ForSys [Bundesministerium für Bildung und Forschung (BMBF)] and by the BioFuture funding of the BMBF. **Author contributions:** S.M., D.U., H.B., R.E., and C.W. designed the research; S.M. and D.U. performed the experiments; S.M., D.U., H.B., R.E., and C.W. analyzed the data; and S.M., D.U., and C.W. wrote the paper. **Competing interests:** The authors declare that they have no competing interests.

Submitted 7 July 2010
Accepted 12 May 2011
Final Publication 31 May 2011
10.1126/scisignal.2001325
Citation: S. Mesecke, D. Urlaub, H. Busch, R. Eils, C. Watzl, Integration of activating and inhibitory receptor signaling by regulated phosphorylation of Vav1 in immune cells. *Sci. Signal.* **4**, ra36 (2011).